XAS Investigations on the Iron−Zinc Center of Purple Acid Phosphatase from Red Kidney Beans

S. Priggemeyer,[†] P. Eggers-Borkenstein,[†] F. Ahlers,[†] G. Henkel,[‡] M. Körner,[§] H. Witzel,[§] H.-F. Nolting,[∥] C. Hermes,[∥] and B. Krebs*,[†]

Anorganisch-Chemisches Institut der Universität Münster, Wilhelm-Klemm-Strasse 8, 48149 Münster, Germany, Fachgebiet Anorganische Chemie/Festkörperchemie der Universität Duisburg, Lotharstrasse 1, 47057 Duisburg, Germany, Institut für Biochemie der Universität Münster, Wilhelm-Klemm-Strasse 2, 48149 Münster, Germany, and European Molecular Biology Laboratory, Hamburg Outstation c/o DESY, Notkestrasse 85, 22607 Hamburg, Germany

Received February 4, 1994[⊗]

X-ray absorption measurements are used to study the iron−zinc center of purple acid phosphatase isolated from red kidney beans. XANES and EXAFS data were taken at the iron and the zinc K-edge of the native enzyme (pH 7) and of the enzyme after addition of phosphate at pH 7 and pH 4. In the native enzyme both the iron and zinc ions are coordinated by five O/N donor ligands. The first shell EXAFS data yield a model with 2.4 O/N at 1.91 Å + 2.6 N/O at 2.10 Å around the iron atom, and 3.4 N/O at 1.97 Å + 1.6 N/O at 2.08 Å around the zinc atom. An iron−zinc distance of 3.96 Å was determined. No evidence for a bridging oxo group (indicated by d_{oxo} ca. 1.8 Å) could be obtained. After addition of phosphate the iron edge shifts to lower and the Zn edge to higher energies. At pH 7 the coordination numbers of iron and zinc increase to six (2.4 N/O at 1.94 Å + 3.6 N/O at 2.12 Å, Fe K-edge, and 4.0 N/O at 1.98 Å + 2.0 N/O at 2.11 Å, Zn K-edge). Since the iron−zinc distance decreases by 0.28 Å to 3.68 Å we propose a bridging coordination mode of phosphate at pH 7. Lowering the pH value to 4 does not affect the binding of phosphate. The features of the higher shell peaks in the Fourier transformed spectra remain essentially unchanged and the iron−zinc distance is maintained (d(Fe−Zn) = 3.69 Å). The ligand atoms in the first shells, however, are more disordered, indicating the involvement of protonation equilibria in the first coordination spheres (2.8 N/O at 1.97 Å and 3.2 N/O at 2.19 Å, Fe K-edge, and 4.7 N/O at 2.05 Å and 1.3 N/O at 2.18 Å, Zn K-edge). These results are checked against structural data from XAS and crystallographic studies of a number of iron and zinc model complexes with mixed ligand environments and structural characteristics similar to those expected for the enzyme samples.

Introduction

Purple acid phosphatases (PAP's) have been isolated from mammals as well as from plants.[1] They comprise a group of basic glycoproteins which exhibit activity at pH 4−6 toward activated phosphoric acid monoesters and anhydrides. Several members of this group have been identified to be iron-dependent metalloenzymes.[2] As determined from EPR,[3] ENDOR,[4] ESEEM,[5] NMR,[6] Mössbauer,[3e,7] EXAFS,[8] and magnetic[9] investigations, the mammalian enzymes from bovine spleen and from porcine uteri (uteroferrin) contain an antiferromagnetically coupled diiron center. In addition one nonbridging tyrosinate

[†] Anorganisch-Chemisches Institut der Universität Münster.
[‡] Fachgebiet Anorganische Chemie/Festkörperchemie der Universität Duisburg.
[§] Institut für Biochemie der Universität Münster.
[∥] EMBL, Hamburg Outstation c/o DESY.
[⊗] Abstract published in *Advance ACS Abstracts,* February 1, 1995.

(1) (a) Que, L., Jr.; True, A. E. *Prog. Inorg. Chem.* **1990**, *38*, 97. (b) Vincent, J. B.; Oliver-Lilley, G. L.; Averill, B. A. *Chem. Rev.* **1990**, *90*, 1447. (c) Doi, K.; Antanaitis, B. C.; Aisen, P. *Struct. Bonding* **1988**, *70*, 1. (d) Sanders-Loehr, J. *Iron Carriers and Iron Proteins*; Loehr, T. M., Ed.; VCH Publishers: Weinheim, Germany, 1989; p 374.

(2) (a) Sundararajan, T. A.; Sarman, P. S. *Biochem. J.* **1945**, *56*, 125. (b) Glomset, J.; Porath, J. *Biochim. Biophys. Acta* **1960**, *39*, 1. (c) Singer, M. F.; Fruton, S. J. *J. Biol. Chem.* **1957**, *229*, 111. (d) Campbell, H. D.; Zerner, B. *Biochem. Biophys. Res. Commun.* **1973**, *54*, 1498. (e) Chen, T. T.; Bazer, F. W.; Cetorelli, J. J.; Pollard, W. E.; Roberts, R. M. *J. Biol. Chem.* **1973**, *248*, 8560. (f) Campbell, H. D.; Dionysius, D. A.; Keough, D. T.; Wilson, B. F.; de Jersey, J.; Zerner, B. *Biochem. Biophys. Res. Commun.* **1978**, *82*, 615.

(3) (a) Antanaitis, B. C.; Aisen, P.; Lilienthal, H. R.; Roberts, R. M.; Bazer, F. W. *J. Biol. Chem.* **1980**, *255*, 11204. (b) Antanaitis, B. C.; Aisen. P. *J. Biol. Chem.* **1982**, *257*, 1855, 5330. (c) Davis, J. C.; Averill, B. A. *Proc. Natl. Acad. Sci. U.S.A.* **1982**, *79*, 4623. (d) Antanaitis, B. C.; Aisen, P.; Lilienthal, H. R. *J. Biol. Chem.* **1983**, *258*, 3166. (e) Averill, B. A.; Davis, J. C.; Burman, S.; Zirino, T.; Sanders-Loehr, J.; Loehr, T. M.; Sage, J. T.; Debrunner, P. J. *J. Am. Chem. Soc.* **1987**, *109*, 3760. (f) Day, E. P.; David, S. S.; Peterson, J.; Dunham, W. R.; Bonvoisin, J. J.; Sands, R. H.; Que, L., Jr. *J. Biol. Chem.* **1988**, *263*, 15561. (g) Dietrich, M.; Münstermann, D.; Suerbaum, H.; Witzel, H. *Eur. J. Biochem.* **1991**, *199*, 105.

(4) Doi, K.; McCracken, J; Peisach, J.; Aisen, P. *J. Biol. Chem.* **1988**, *263*, 5757.

(5) Antanaitis, B. C.; Peisach, J.; Mims, W. B.; Aisen, P. *J. Biol. Chem.* **1985**, *260*, 4672.

(6) (a) Lauffer, R. B.; Antanaitis, B. C.; Aisen, P.; Que, L., Jr. *J. Biol. Chem.* **1983**, *258*, 14212. (b) Scarrow, R. C.; Pyrz, J. W.; Que, L., Jr. *J. Am. Chem. Soc.* **1990**, *112*, 657. (c) Wang, Z.; Ming L.-J.; Que, L., Jr.; Vincent, J. B.; Crowder, M. W.; Averill, B. A. *Biochemistry* **1992**, *31*, 5263. (d) Holz, R. C.; Que, L., Jr.; Ming, L.-J. *J. Am. Chem. Soc.* **1992**, *114*, 4434.

(7) (a) Debrunner, P. G.; Hendrich, M. P.; de Jersey, J.; Keough, D. T.; Sage, J. T.; Zerner, B. *Biochim. Biophys. Acta* **1983**, *745*, 103. (b) Pyrz, J. W.; Sage, J. T.; Debrunner, P. G.; Que, J., Jr. *J. Biol. Chem.* **1986**, *261*, 11015. (c) Cichutek, K.; Witzel, H.; Parak, F. *Hyperfine Interactions* **1988**, *42*, 885. (d) Sage, J. T.; Xia, Y.-A.; Debrunner, P. J.; Keough, D. T.; de Jersey, J.; Zerner, B. *J. Am. Chem. Soc.* **1989**, *111*, 7239.

(8) (a) Kauzlarich, S. M.; Teo, B.-K.; Zirino, T.; Burman, S.; Davis, J. C.; Averill, B. A. *Inorg. Chem.* **1986**, *25*, 2781. (b) Que, L., Jr.; Scarrow R. C. *Metal Clusters in Proteins*; ACS Symposium Series 372, American Chemical Society: Washington DC, 1988; p 152. (c) True, A. E.; Scarrow, R. C.; Holz, R. C.; Que, L., Jr. *J. Inorg. Biochem.* **1991**, *43*, 545. (d) True, A. E.; Scarrow, R. C.; Randall, C. R.; Holz, R. C.; Que, L., Jr. *J. Am. Chem. Soc.* **1993**, *115*, 4246.

(9) (a) Mockler, G. M.; de Jersey, J.; Zerner, B.; O'Connor, C. J.; Sinn, E. J. *J. Am. Chem. Soc.* **1983**, *105*, 1891. (b) Sinn, E.; O'Connor, C. J.; de Jersey, J.; Zerner, B. *Inorg. Chim. Acta* **1983**, *78*, L13. (c) Gehring, S.; Fleischhauer, P.; Haase, W.; Dietrich, M.; Witzel, H. *Biol. Chem. Hoppe-Seyler* **1990**, *371*, 786.

0020-1669/95/1334-1445$09.00/0 © 1995 American Chemical Society

residue as well as histidine residues bound to each of the metal ions are present.

The purple color of the PAP's has been attributed to tyrosinate-to-iron(III) charge transfer transitions which give rise to a broad absorption band between 510 and 560 nm and the characteristic phenoxide ring modes in the resonance Raman spectra.[3e,10]

The mammalian PAP's from beef spleen and porcine uteri are stable in two interconvertible species: a highly active, pink Fe(II)−Fe(III) form and an oxidized, purple Fe(III)−Fe(III) state with low phosphatase activity.[3e,g] They can be distinguished readily by means of EPR spectroscopy.

To date, PAP's originating from plants have been characterized to a much lesser extent. During the last decade, however, several reports appeared describing the isolation of transition metal dependent acid phosphatases from sweet potatoes,[11] kidney beans,[12] soy beans,[13] spinach,[14] and rice.[15] In contrast to their mammalian counterparts, the majority of these enzymes consists of two subunits. Their molecular weights are considerably higher (ca. 110 kDa) as compared to the monomeric mammalian enzymes (35 kDa). Metal analyses and EPR spectra indicated the presence of manganese.

The enzyme from kidney beans is unique because of its zinc content and it is an interesting example of a naturally occurring zinc−iron metalloenzyme containing an Fe(III)−tyrosinate moiety. With respect to kinetic and physicochemical properties it closely resembles the reconstituted active zinc−iron derivatives of the bovine spleen and uterine phosphatases.[16]

On the other hand, Zn(II) can be replaced in the kidney bean enzyme by Fe(II).[12,17] This derivative now resembles the spleen enzyme and uteroferrin. Its inactive Fe(III)−Fe(III) species does not give an EPR signal, the active Fe(III)−Fe(II) species again shows a signal at $g_{av} = 1.75$, in contrast to the native Fe(III)−Zn(II) species with an Fe(III) high spin signal at $g = 4.3$ and 9.2.[12d] The Mössbauer data agree very well with those for the mammalian enzymes.[17] A significant difference is found in the visible spectrum of the Fe(III)−Fe(II) kidney bean enzyme where the absorption maximum of the CT-band shifts from 558 to 565 nm and not to 515 nm as observed in both mammalian enzymes upon reduction.[17]

Specific information on the interaction of PAP's is obtained from reaction studies of the active centers with the natural substrates and with tetrahedral oxo anions, especially with phosphate, as substrate models. On the basis of the pH dependence of kinetic and spectroscopic data a primary interaction of the ester phosphate group with Fe(II) has been postulated followed by an attack of an OH-ligand at the Fe(III) in an S_N2 type reaction.[3g] This is in agreement with the inversion of the absolute configuration at the phosphorus.[18] An enzyme-bound imidazolyl phosphate intermediate thus is less likely.[19] Furthermore, stopped flow measurements on uteroferrin showed that the ester substrates as well as the inhibiting phosphate oxoanions interact first with Fe(II). This is followed by formation of the bridge to Fe(III) in a slower step.[20] These studies indicate that phosphate forms a bidentate bridge between the two metal ions.

NMR studies on uteroferrin and bovine spleen PAP lead to an updated model for the Fe(III)−Fe(II) center with both metals in a pentacoordinated environment.[6c] There is direct evidence for a tyrosine and histidine ligand at the Fe(III) site. The coordination sphere then should be completed by a water molecule. In addition a carboxylato group in the coordination sphere of the metal−metal site is postulated. The EXAFS studies of True et al. support this model.[8d] No evidence was found for a μ-oxo bridge, which would require a scatterer at ca. 1.8 Å. The sixth coordination site at the irons should be occupied by aqua ligands. A low-Z scatterer at 2.4 Å is assigned to the chelating carboxylate group at Fe(II) in accordance with NOSY studies on the Fe(III)−Co(II) species.[6d] The Fe−Fe distance of the reduced Fe(III)−Fe(II) species is 3.52 Å; in the oxidized species and in the presence of phosphate the Fe−Fe distance is shortened to an average distance of 3.2 Å.

The present EXAFS study on kidney bean PAP was performed in order to obtain specific structural information on the active site in the absence of a full single crystal structure study.[21] Additional attention is given to the interaction of the kidney bean enzyme and the model compounds with phosphate as substrate model.

As compared to the previous EXAFS studies on the inactive oxidized forms of bovine spleen and porcine uterine Fe(III)−Fe(III) PAP's, these studies showed that kidney bean phosphatase offers the unique opportunity to study the individual metal sites of the two-metal unit separately.

Experimental Section

Sample Preparation. Purple Acid Phosphatase. The purple acid phosphatase from red kidney beans was isolated and purified by a slightly modified procedure originally given by Zerner et al.[12b] The isolated homogeneous KBPase in 0.5 M NaCl was concentrated and NaCl was exchanged for 0.5 M $LiNO_3$ by ultrafiltrating several times. The dark purple concentrate was centrifuged to remove denatured protein. The enzyme solution was stabilized by adding 10% glycerol. Three enzyme samples were prepared: native enzyme, adjusted to pH

(10) (a) Gaber, B. P.; Sheridan, J. P.; Bazer, F. W.; Roberts, R. M. *J. Biol. Chem.* **1979**, *254*, 8340. (b) Antanaitis, B. C.; Strekas, T.; Aisen, P. *J. Biol. Chem.* **1982**, *257*, 3766.

(11) (a) Uehara, K.; Fujimoto, S.; Taniguchi, T. *J. Biochem.* **1971**, *70*, 183. (b) Uehara, K.; Fujimoto, S.; Taniguchi, T. *J. Biochem.* **1974**, *75*, 627. (c) Fujimoto, S.; Ohara, A.; Uehara, K. *Agric. Biol. Chem.* **1980**, *44*, 1659. (d) Sugiura, Y.; Kawabe, H.; Tanaka, H.; Fujimoto, S.; Okara, A. *J. Biol. Chem.* **1981**, *256*, 10664. (e) Kawabe, H.; Sugiura, Y.; Terauchi, M.; Tanaka, H. *Biochim. Biophys. Acta* **1984**, *784*, 81. (f) Hefler, S. K.; Averill, B. A.; *Biochem. Biophys. Res. Commun.* **1987**, *146*, 1173.

(12) (a) Nochumson, S.; O'Rangers, J. J.; Dimitrov, N. V. *Fed. Proc.* **1974**, *33*, 1378. (b) Beck, J. L.; McConachie, L. A.; Summors, A. C.; Arnold, W. N.; De Jersey, J.; Zerner, B. *Biochim. Biophys. Acta* **1986**, *869*, 61. (c) Beck, J. L.; De Jersey, J.; Zerner, B.; Hendrich, M. P.; Debrunner, P. J. *J. Am. Chem. Soc.* **1988**, *110*, 3317. (d) Beck, J. L.; McArthur, M. J.; de Jersey, J.; Zerner, B. *Inorg. Chim. Acta* **1988**, *153*, 39.

(13) (a) Fujimoto, S.; Nakagawa, T.; Ishimitsu, S.; Ohara, A. *Chem. Pharm. Bull.* **1977**, *25*, 3283. (b) Fujimoto, S.; Nakagawa, T.; Ishimitsu, S.; Ohara, A. *Agric. Biol. Chem.* **1977**, *41*, 599. (c) LeBansky, B. R.; McKnight, T. D.; Griffing, L. R. *Plant Physiol.* **1992**, *99*, 391.

(14) Fujimoto, S.; Nakagawa, T.; Ishimitsu, S.; Ohara, A. *Chem. Pharm. Bull.* **1977**, *25*, 1459.

(15) Igaue, I.; Watabe, H.; Takahashi, K.; Takekoshi, M.; Morota, A. *Agric. Biol. Chem.* **1976**, *440*, 823.

(16) (a) Keough, D. T.; Dionysius, D. A.; de Jersey, J.; Zerner, B. *Biochem. Biophys. Res. Commun.* **1980**, *94*, 600. (b) Davis, J. C.; Averill, B. A. *Proc. Natl. Acad. Sci. U.S.A.* **1982**, *79*, 4623. (c) David, S. S.; Que, L., Jr. *J. Am. Chem. Soc.* **1990**, *112*, 6455.

(17) Suerbaum, H.; Körner, M.; Witzel, H.; Althaus, E.; Mosel, B.-D.; Müller-Warmuth, W. *Eur. J. Biochem.* **1993**, *214*, 313.

(18) Mueller, E. G.; Crowder, M. W.; Averill, B. A.; Knowles J. R. *J. Am. Chem. Soc.* **1993**, *115*, 2974.

(19) (a) Vincent, J. B.; Crowder, M. W.; Averill, B. A. *Biochemistry* **1991**, *30*, 3025. (b) Vincent, J. B.; Crowder, M. W.; Averill, B. A. *J. Biol. Chem.* **1991**, *266*, 17737.

(20) (a) Aquino, M. A. S.; Lim, J.-S.; Sykes, A. G. *J. Chem. Soc., Dalton Trans.* **1992**, 2135. (b) Aquino, M. A. S.; Lim, J.-S.; Sykes, A. G. *J. Chem. Soc., Dalton Trans.* **1994**, 429.

(21) First results on crystals from the kidney bean PAP were published by: Sträter, N.; Fröhlich, R. Schiemann, A.; Krebs, B.; Körner, M.; Suerbaum, H.; Witzel, H. *J. Mol. Biol.* **1992**, *224*, 511.

(22) Both the iron and zinc K-edges of the enzyme samples and of the heterodinuclear model compounds were analyzed independently. Consequently, the extension **-Fe** is used for data obtained from the Fe K-edge while the extension **-Zn** is used for the Zn K-edge.

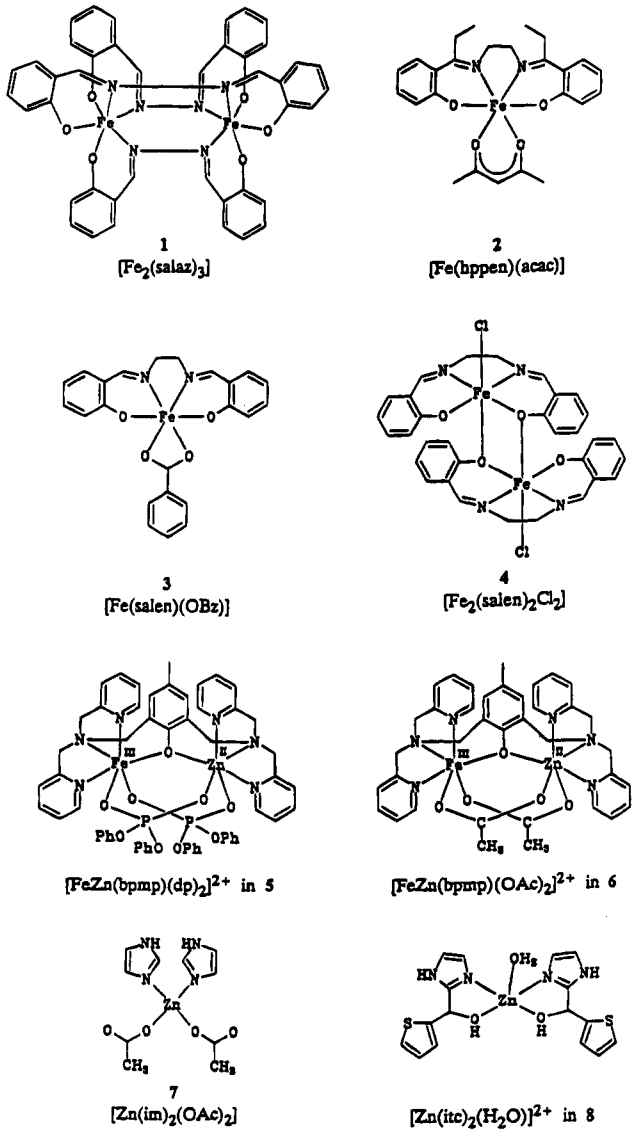

Figure 1. Structural formulas of the model compounds.

7.0 (3.3 mmol), **PAP7**;[22] native enzyme in 0.1 M phosphate, pH 7.0 (3.8 mmol), **PAP7P**;[22] native enzyme in 0.1 M phosphate, pH 4.0 (3.2 mmol), **PAP4P**.[22]

The protein concentrations given in parentheses were determined by quantitative analysis of the absorbance at the visible absorption maximum (ϵ_{560} = 6480 M^{-1} cm^{-1}).

Model Compounds. The compounds are depicted in Figure 1. The numbers and types of scatterers (cn) and the corresponding mean absorber–scatterer distances (R) of the model compounds—except for compound **3** which is only used in the discussion of the XANES spectra—are summarized in Table 1.

$[Fe_2(salaz)_3]$ (**1**) (H_2salaz = bis(salicylidene)hydrazine) was prepared (a) by reaction of *N,N'*-bis(salicylidene)-1,8-diamino-3,6-dithiaoctane (H_2salddto) with $Fe(OAc)_2$ in DMF/methanol, involving reductive cleavage of H_2salddto followed by complex formation with the resulting H_2salaz, or (b) by reaction of $FeCl_3$ and H_2salaz in methanol.[23] The molecular structure was obtained from single crystal X-ray diffraction on black crystals of **1**·MeOH (refined to R = 0.032).[23]

[Fe(hppen)(acac)] (**2**) (H_2hppen = (*N,N'*-ethylenebis(*o*-hydroxypropiophenone imine)) was synthesized by reacting H_2hppen (4.6 mmol) with $Fe(acac)_3$ (0.5 mmol) in a 3:1 MeOH/$CHCl_3$ mixture (30 mL).[24] The ligand H_2hppen was obtained from *o*-hydroxypropiophenone (20 mmol) and ethylenediamine (10 mmol) in boiling MeOH (20 mL). The crystal structure of **2** was refined to R = 0.053.[24]

[Fe(salen)(OBz)] (**3**) (H_2salen = *N,N'*-bis(salicylidene)ethylenediamine, HOBz = benzoic acid) was prepared by a modification of the classic synthesis,[25] reacting HOBz in EtOH with $[Fe(salen)_2O]$·2pyridine. Recrystallization from $CHCl_3$ yielded black crystalline [Fe(salen)(OBz)]·$CHCl_3$.[23] The crystal structure was refined to R = 0.034.[23]

$[Fe_2(salen)_2Cl_2]$ (**4**),[26] $[FeZn(bpmp)(dp)_2]^{2+}$ in $[FeZn(bpmp)(dp)_2](ClO_4)_2$·1.5MeOH·$H_2O$ (**5**)[22] (Hbpmp = 2,6-bis[bis(2-pyridylmethyl)-aminomethyl]-4-methylphenol, Hdp = diphenylphosphoric acid),[27] $[FeZn(bpmp)(OAc)_2]^{2+}$ in $[FeZn(bpmp)(OAc)_2](BPh_4)_2$·MeCN (**6**)[22] (HOAc = acetic acid),[28] and $[Zn(im)_2(OAc)_2]$ (**7**) (im = imidazole)[29] were prepared according to published procedures, and single crystal X-ray diffraction data were taken from the same sources.

$[Zn(itc)_2(H_2O)]^{2+}$ (itc = (imidazole-2-yl-thiophene-2-yl)carbinol)) was prepared at 60 °C by reaction of itc (2.8 mmol) in 30 mL of methanol/acetone with 1.4 mmol of $ZnSO_4$·$7H_2O$ in 20 mL of methanol/H_2O (1:1). Recrystallization from DMF yielded crystals of $[Zn(itc)_2(H_2O)](SO_4)$·H_2O·10DMF (**8**).[30] The crystal structure was refined to R = 0.062.[30]

X-ray Absorption Measurements. X-ray absorption spectra at the Fe and Zn K-edge were recorded at the European Molecular Biology Laboratory (c/o DESY, Hamburg) using the synchrotron radiation from storage ring DORIS II.[31] Data collection was performed under dedicated conditions at ca. 3.7 GeV and 50–100 mA (enzyme samples) and at ca. 5.3 GeV and 20–50 mA (model compounds). A Si(220) double crystal monochromator was used with a typical energy resolution

Table 1. Structural Parameters of the Model Compounds

sample	shell	no. and type of scatterer	R_{av} (Å)
1	I	3 O	1.919
		3 N	2.171
	II	6 C	3.038
	III	1 Fe	3.926
2	I	2 O	1.915
		2 O, 2 N	2.084
4	I	1 O	1.897
		2 O, 2 N	2.087
		1 Cl	2.295
	II	7 C	3.015
	III	1 Fe	3.290
5-Fe	I	3 O	1.993
		3 N	2.135
	II	8 C	3.017
	III	2 P	3.232
	IV	1 Zn	3.695
5-Zn	I	2 O	2.046
		1 O, 3 N	2.151
	II	8 C	3.017
	III	2 P	3.268
	IV	1 Fe	3.695
6-Fe	I	2 O	1.960
		1 O, 3 N	2.130
	II	10 C	3.018
	III	1 Zn	3.436
6-Zn	I	1 O	1.999
		2 O, 3 N	2.117
	II	10 Cl	3.014
	III	1 Fe	3.436

(23) Nienaber, P.; Krebs, B. Unpublished work. Nienaber, P. Ph.D. Dissertation, University of Münster, 1985.
(24) Bremer, B.; Krebs, B. Unpublished work. Bremer, B. Diploma Thesis, University of Münster, 1988.
(25) Pfeiffer, P.; Breith, E.; Lübbe, E.; Tsumaki, T. *Liebigs Ann. Chem.* **1933**, *503*, 84.
(26) Gerloch, M.; Mabbs, F. E. *J. Chem. Soc. A* **1967**, 1900.
(27) Schepers, K.; Bremer, B.; Krebs, B.; Henkel G.; Althaus, E.; Mosel, B.; Müller-Warmuth, W. *Angew. Chem.* **1990**, *102*, 582; *Angew. Chem., Int. Ed. Engl.* **1990**, *29*, 531.
(28) Borovik, A. S.; Papaefthymiou, V.; Taylor, L. F.; Anderson, O. P.; Que, Jr., L. *J. Am. Chem. Soc.* **1989**, *111*, 6183.
(29) Horrocks, Jr., W. D.; Ishley, J. N.; Whittle, R. R. *Inorg. Chem.* **1982**, *21*, 3265.
(30) Kirchner, C.; Simonis, U.; Krebs, B. Unpublished work. Kirchner, C. Ph.D. Dissertation, University of Münster, 1987.
(31) (a) Hermes, C.; Gilberg, E.; Koch, M. H. J. *Nucl. Instrum. Methods* **1984**, *222*, 207. (b) Pettifer, R. F.; Hermes, C. *J. Appl. Crystallogr.* **1985**, *18*, 404. (c) Pettifer, R. F.; Hermes, C. *J. Phys. (Paris)* **1986**, *C8*, 127.

of 1.5 eV.[31b] Harmonic rejection was accomplished by detuning the first monochromator crystal by 50%. The spectra were recorded at 20 K using a modified Oxford Instruments cryostat over the energy range from 6600 to 8200 eV for the Fe K-edge and from 9200 to 11000 keV for the Zn K-edge, respectively.

X-ray absorption spectra for the model compounds were collected in transmission by using ionization chambers (Ar/CO_2). These samples were prepared according to ref 32 . At least two individual spectra were recorded for each sample to check for reproducibility and to improve counting statistics.

The spectra of the protein solutions were obtained by counting the emitted fluorescence photons with plastic scintillation detectors. The samples were enclosed in appropriate cells with kapton foil windows. For each protein sample about 15−20 individual scans were recorded.

Data Analysis. A calibration procedure was used to rescale the energy axis of the spectrometer to absolute values with a number of Bragg reflections obtained from an oriented Si crystal.[31b] The average value ot the individual scans for each sample were used for analysis. The resulting spectrum was first corrected for a monotonically decreasing background function caused by the other elements present and higher shell absorption processes of the absorber. These background contributions were approximated by a least-squares fit of Victoreen's formula[33] (absorption measurements) or a second order polynomial (fluorescence measurements) to the preedge data range and subtracted from the spectrum.

The preedge peak area was calculated by subtracting an arctangent function from the normalized edge spectrum and integrating over a range of ca. 10 eV. The edge position was defined as the first inflection point of the normalized XANES and determined from the derivative spectrum.

The EXAFS function $\chi(E)$ was derived from the corrected absorption spectrum and subsequently converted into photoelectron wave vector space $\chi(k)$ according to

$$k = \sqrt{\frac{8\pi^2 m(E - E_0)}{h^2}}$$

where m is the electron rest mass and E_0 is the energy threshold of the Zn or Fe K-edge. It is not possible to determine E_0 experimentally, because there is no characteristic feature in an XAS spectrum which can be assigned directly to the threshold energy. In this work we used 7120.0 eV for the Fe and 9660.0 eV for the Zn K-edge to define E_0 for the data reduction. Residual inaccuracies of the threshold energy are modeled by ΔE_0 in the curve-fitting analyses.

The $\chi(k)$ values were multiplied by k^3 and transformed by Fourier procedures using different square windows. Except where otherwise stated, the Fourier transform range is 3.0−11.5 $Å^{-1}$ for the enzyme samples and 3.0−16.5 $Å^{-1}$ for the model compounds. Prior to curve-fitting analyses, the individual peaks in these functions were back-transformed into single-shell EXAFS spectra according to the Fourier filtering approach. The individual window widths used in the various calculations are listed in Tables 3−5.

The Fourier-filtered spectra were refined with least-squares techniques based on single-scattering EXAFS theory using theoretical amplitude ($F(k)$) and phase functions ($\Phi(k)$)[34] according to:

$$\chi(k) = \sum_s S_0^2 \frac{N_s k_m^2}{R_s^2} F(k_m) e^{-2\sigma_s^2 k_m^2} e^{-2R_s \eta / k_m} \sin[2k_m R_s + \phi(k_m)]$$

$$k_m = \sqrt{k^2 - 0.2625\Delta E_0}^T$$

where s denotes the number of (sub)shells to be fitted. For each shell the number of scatterers (N_s), the absorber−scatterer distance (R_s) and the mean square displacements (σ_j^2) can be refined. Additionally, for each different absorber−scatterer pair, ΔE_0 (used to define k) can be varied.

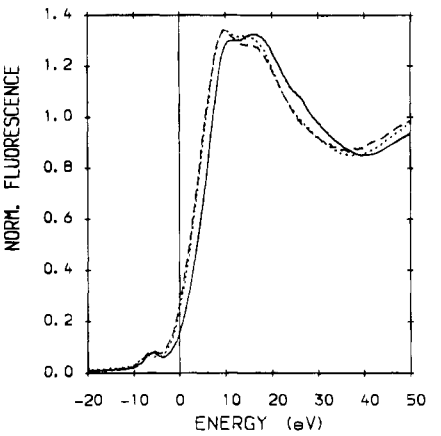

Figure 2. Iron K-edge spectra of **PAP7-Fe** (—), **PAP7P-Fe** (···), **PAP4P-Fe** (— —). Energy zero at 7120.0 eV.

Furthermore, we used 0.8 for the amplitude reduction factor S_0^2 and 4 eV for the inelastic loss parameter η.[35]

The goodness of fit is given as $RF = (\Sigma[\chi(k)_{obs} - \chi(k)_{calc}]^2)/(\Sigma[\chi(k)_{obs}]^2)$. The maximum number of parameters allowed to vary simultaneously in the curve fitting analyses were estimated by $N_{free} = 2\Delta R_{FF}\Delta k_{fit}/\pi$ where ΔR_{FF} is the width of the filter window and Δk_{fit} is the length of the data set in k space.

Results

Near Edge Structure. Figures 2 and 3 show the XANES spectra of the different kidney bean PAP preparations and of representative model compounds at the iron and zinc K-edge, respectively. The numerical values of the edge positions are summarized in Table 2. The iron edge positions of the native enzyme is at 6.6 eV (**PAP7-Fe**), which is consistent with Fe(III) coordinated by N/O-donor ligands.[36] Upon addition of phosphate, the iron edge positions shift to lower energies by ca. 2 to 4.4 eV for **PAP7P-Fe** and to 4.2 eV for **PAP4P-Fe**. These shifts are not due to photoreduction of the Fe(III) sites as observed for methane monooxygenase[37] since (i) the enzyme samples exhibit the same activity before and after data collection and (ii) no shift in the iron edge positions of the individual scans was observed in the period during data collection. It is most likely that these shifts originate from the interaction of the phosphate anion(s) with the dimetal core.

The corresponding edge positions at the zinc K-edge are 5.3 (**PAP7-Zn**), 5.7 (**PAP7P-Zn**), and 6.4 eV (**PAP4P-Zn**). These values are typical for Zn with O/N ligands.[38] It is striking that the zinc edge positions are shifted in the opposite direction to the corresponding iron edge positions.

The most interesting feature of the iron K-edge spectrum is the 1s → 3d transition at ca. 6 eV below E_0 (E_0 = 7120.0 eV). This transition is forbidden according to selection rules but occurs due to quadrupole and symmetry-breaking effects. Roe et al. demonstrated that the preedge peak intensities of various Fe(III) model compounds vary inversely with the coordination number.[39] The preedge peak intensities of the compounds under

(32) Nolting, H.-F.; Tremel, W.; Eggers, P.; Henkel, G.; Krebs, B. *Nucl. Instrum. Methods Phys. Res. A* **1987**, *259*, 576.
(33) Victoreen, J. A. *J. App. Phys.* **1948**, *19*, 855.
(34) McKale, A. G.; Veal, B. W.; Paulikas, A. P., Chan, S.-K.;Knapp, G. S. *J. Am. Chem. Soc.* **1988**, *110*, 3763.
(35) Pettifer, R. F. *Characterization of Catalysts*; Thomas, J. M., Lambert, R. M., Eds.; Wiley: Chichester, England, 1980; pp 264−273.
(36) (a) Priggemeyer, S. Ph.D. Dissertation, University of Münster 1991. (b) Priggemeyer, S.; Krebs, B.; Henkel, G. Unpublished results.
(37) Ericson, A.; Hedman, B.; Hodgson, K. O.; Green, J.; Dalton, H.; Bentson, J. G.; Beer, R. H.; Lippard, S. J. *J. Am. Chem. Soc.* **1988**, *110*, 2330.
(38) (a) Eggers-Borkenstein, P. Ph.D. Dissertation, University of Münster, 1989. (b) Eggers-Borkenstein, P.; Krebs, B.; Henkel, G. Unpublished results.

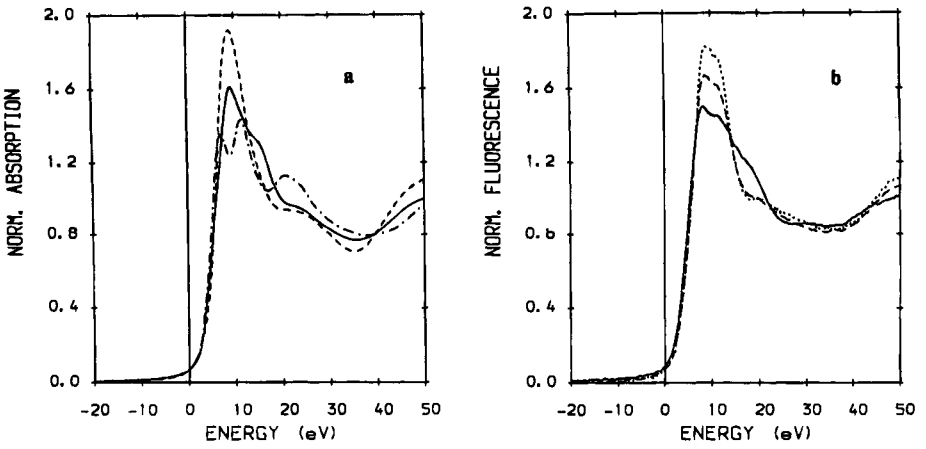

Figure 3. Zinc K-edge spectra of **7** (a, – • –), **8** (a, —), **5-Zn** (a, – –), **PAP7-Zn** (b, —), **PAP7P-Zn** (b, – –) and **PAP4P-Zn** (b, • • •). Energy zero at 9660.0 eV.

Table 2. Iron and Zinc K-Edge Data

sample	donor atoms	edge position[a] (eV)	1s → 3d peak area
PAP7-Fe	5N/O[b]	6.6	0.129
PAP7P-Fe	6N/O[b]	4.4	0.099
PAP4P-Fe	6N/O[b]	4.5	0.116
1	3N, 3O	5.3	0.067
2	2N, 4O	5.8	0.074
3	2N, 4O	4.4	0.101
4	2N, 3O, 1Cl	3.8	0.068
5-Fe	3N, 3O	4.5	0.068
6-Fe	3N, 3O	3.3	0.060
PAP7-Zn	5N/O[b]	5.3	
PAP7P-Zn	6N/O[b]	5.7	
PAP4P-Zn	6N/O[b]	6.4	
5-Zn	3N, 3O	6.3	
6-Zn	3N, 3O	6.3	
7	2N, 2O	5.2	
8	2N, 3O	4.7	

[a] Defined as the first maximum in the first derivative of the normalized edge spectra; energy zero at 7120.0 eV and 9660.0 eV, respectively. [b] This work

investigation are included in Table 2. Figure 4 shows that in principle each coordination number corresponds to a characteristic range of peak areas.

The preedge peak intensity of **PAP7P-Fe** (0.099 unit) falls into the range of areas obtained for six-coordinated Fe(III) model complexes indicating a distorted octahedral coordination for the iron site. On the other hand **PAP7-Fe** gives rise to a peak area which falls into the lower region of pentacoordinated model compounds (0.129 unit) and is thus indicative for a 5-fold coordination. From this correlation, however, there is some ambiguity with respect to the coordination number of **PAP4P-Fe**. To make a correct assignment, we analyzed the Fourier transformed fine structure. In general, the first shell peak is less intense and broader for more distorted first coordination spheres than for less distorted coordination environments. The first shell peak in the Fourier transformed spectrum of **PAP4P-Fe** (Figure 6) is very broad and already split into two subpeaks. Therefore, a distorted octahedral geometry can be assumed for the iron atom in **PAP4P-Fe**. By comparison, other iron enzymes, e.g. catechol 1,2-dioxygenase and protocatechuate 3,4-dioxygenase, give rise to similar preedge peak areas. The active sites of these enzymes were also interpreted to be six-coordinated with a weakly bound sixth ligand.[39]

Due to its d^{10} configuration, zinc does not exhibit a preedge peak. Nevertheless, information about the coordination geometry of the zinc absorber atom can be obtained by comparing the features of the XANES spectra of the enzyme samples with those of model compounds. The XANES spectra of **7**, **8**, and **5-Zn** are representative for Zn with O/N ligands and tetrahedral (**7**), trigonal-bipyramidal (**8**) and octahedral (**5-Zn**) coordination. Figure 3 shows a great similarity between the XANES spectra of **PAP7-Zn** and of the penta-coordinated complex **8**. On the other hand, the edge features of the enzyme samples after addition of phosphate (**PAP7P-Zn** and **PAP4P-Zn**) resemble those of the six-coordinate compound.

The results described above show that after addition of phosphate anions structural changes within the first coordination sphere occur at both the iron and zinc site of the dinuclear center.

Extended X-ray Absorption Fine Structure. As an example, the k^3-weighted EXAFS data of the protein samples at the iron K-edge are presented in Figure 5. Again, a difference between the spectrum of the native enzyme and the spectra of the two species in the presence of phosphate can be seen. Figure 6 shows the Fourier transforms of the k^3-weighted fine structures of the native kidney bean PAP and the two enzyme–phosphato complexes at the Fe K-edge. Figure 7 presents the corresponding spectra at the Zn K-edge.

The data of the native enzyme show peaks arising from scattering atoms in the first, second and third shells of iron and zinc. Addition of phosphate causes significant changes in the shape of the higher shell contributions in the Fourier transform. For example, the peak at 2.9 Å in the Fourier transform of **PAP7-Fe** is split into two components at 2.5 and 3.1 Å and the peak at 3.7 Å is shifted toward lower R values (**PAP7P-Fe** and **PAP4P-Fe** in Figure 6). Decreasing the pH after addition of phosphate does not result in fundamental changes of the higher shell contributions to the Fourier transform but greater distortion of the first shell in **PAP4P-Fe** is observed. The Fourier transforms of the enzyme samples at the zinc K-edge show analogous characteristics.

First Shell. Iron K-Edge. Fourier-filtered EXAFS data of the first shell were used in curve-fitting analyses, with window widths as indicated in Table 3. A single shell fit (backscatterer O/N) could not adequately fit the first shell EXAFS data for any of the samples under investigation. Therefore, fits were performed using an oxygen and a nitrogen subshell. EXAFS spectroscopy can not distinguish between backscatteres of similar atomic number (e.g. N and O), thus subshell 1 was modeled as a shell of cn_O oxygen atoms while subshell 2 was modeled by cn_N nitrogen atoms. Since M–N bonds (M = Fe, Zn) are usually longer than M–O bonds, fits with $R_N > R_O$ were performed (R_N and R_O refer to the initial bond lengths).

(39) Roe, A. L.; Schneider, D. J.; Mayer, R. J.; Pyrz, J. W.; Widom J.; Que, L., Jr. *J. Am. Chem. Soc.* **1984**, *106*, 1676.

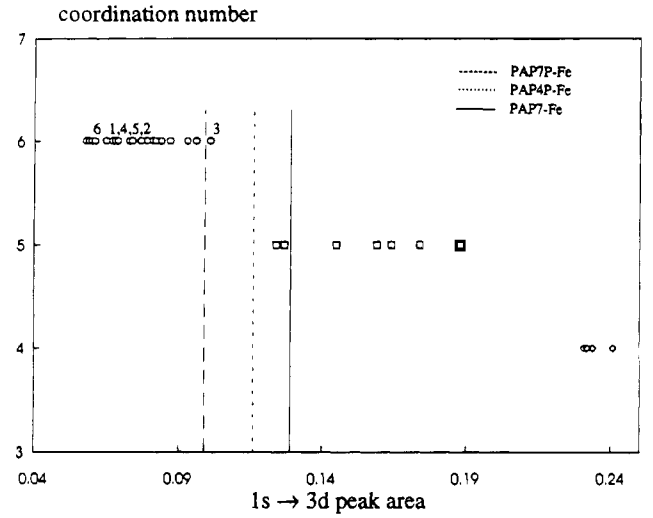

Figure 4. Coordination number vs 1s → 3d peak area: (○) six-coordinate compounds; (□) five-coordinate compounds; (◇) four-coordinate compounds. Values taken from Table 2 and ref 39.

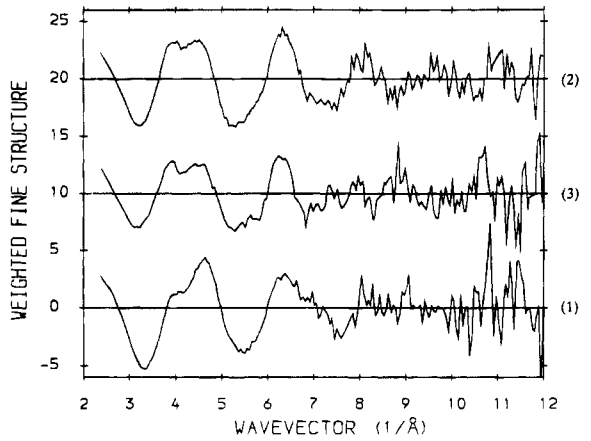

Figure 5. k^3-weighted fine structure at the Fe K-edge of **PAP7-Fe** (1), **PAP7P-Fe** (2), and **PAP4P-Fe** (3).

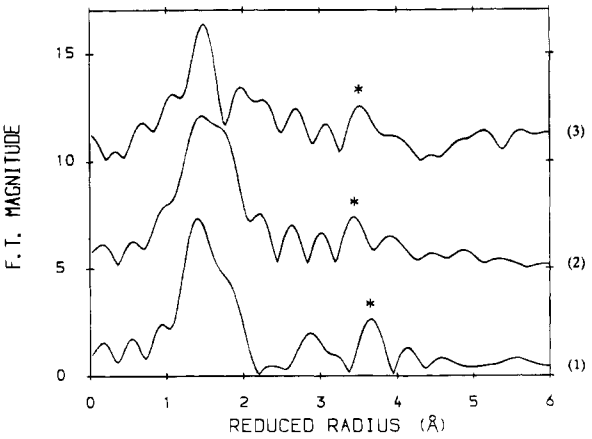

Figure 6. Fourier transform of the k^3-weighted fine structure (Fe K-edge) of **PAP7-Fe** (1), **PAP7P-Fe** (2), and **PAP4P-Fe** (3).

Though the number of free variables does not exceed the maximum number of adjustable parameters N_{free}, two-subshell fits to the first shell EXAFS data of the enzyme samples at the iron K-edge varying ΔE_0,[40] cn_O, cn_N, R_O, R_N, σ^2_O, and σ^2_N gave no reasonable results because of high correlations between variables within and between the subshells. Systematic analyses

(40) Since the amplitude and phase functions of oxygen and nitrogen are very similar, only one ΔE_0 was allowed to vary.

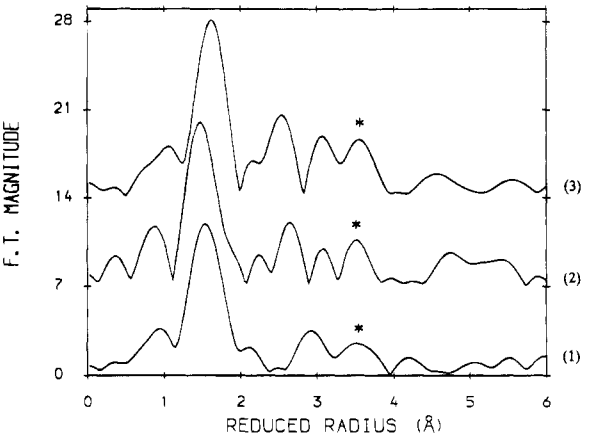

Figure 7. Fourier transform of the k^3-weighted fine structure (Zn K-edge) of **PAP7-Zn** (1), **PAP7P-Zn** (2), and **PAP4P-Zn** (3).

Table 3. Results of Curve Fitting Analysis of the First Shell EXAFS Data of the Kidney Bean PAP and of Model Compounds (Fe K-Edge)

sample	window width (Å)	N_{free}[a]	scatterer	cn[b]	R (Å)	$10^3\sigma^2$ (Å^2)	ΔE_0 (eV)	RF[a] (%)
PAP7-Fe	0.9−2.1	7	O	2.4	1.91[c]	4.4	6.7	14.1
			N	2.6	2.10	3.2		
PAP7P-Fe	0.9−2.1	7	O	2.4	1.94[d]	5.5	6.5	18.4
			N	3.6	2.12	4.1		
PAP4P-Fe	1.0−2.2	7	O	2.8	1.97[d]	8.1	7.0	19.1
			N	3.2	2.19	4.0		
1	1.1−2.2	10	O	2.9	1.92	2.2	5.4	18.8
			N	2.6	2.19	4.5		
2	1.0−2.1	8	O	1.5	1.93[e]	2.2	6.2	12.9
			N	4.5	2.08	5.7		
5-Fe	1.1−2.1	9	O	3.0	1.95[f]	3.8	5.6	18.0
			N	3.0	2.15			
6-Fe	1.0−2.1	10	O	2.1	1.94[g]	3.2	6.0	24.3
			N	3.9	2.14	7.0		

[a] As defined in the Experimental Section. [b] cn = coordination number. [c] R_{av} = 2.00 Å and Σcn = 5. [d] R_{av} = 2.06 Å and Σcn = 6. [e] R_{av} = 2.03 Å and Σcn = 6. [f] R_{av} = 2.05 Å and Σcn = 6.[28] [g] R_{av} = 2.07 Å and Σcn = 6.[28]

of suitable model compounds show that in these cases reliable fit results can be obtained by keeping the mean absorber−scatterer distance of the first shell ($R_{av} = (cn_N R_N + cn_O R_O)/(cn_N + cn_O)$),[41] and the overall number of scatterers in the first shell (Σcn) constant.[36] For example, compound **2**, **5-Fe**, and **6-Fe** show correlations similar to those found for the enzyme samples.[42] The first shell EXAFS data of these complexes were fitted with a two-subshell model varying ΔE_0, cn_O, R_O, σ^2_O, and σ^2_N. cn_N and R_N were calculated within the fit procedure according to $cn_N = \Sigma cn - cn_O$ and $R_N = ((cn_N + cn_O)R_{av} + cn_O R_O)/cn_N$. It is evident from Table 3 that this procedure yields absorber−scatterer distances which are accurate within ±0.04 Å, whereas the errors of the coordination numbers are about ±0.5 atom.

R_{av} and Σcn were extracted for the enzyme samples from the XANES spectra via comparison of characteristic features of the edge spectra with those of model compounds:[36] Comparison of the preedge peak intensities yields the overall number of scatterers Σcn (see above). R_{av} was determined by analyzing

(41) cn_O and cn_N refer to the initial number of scatterers.

(42) For example, the correlation coefficients for a two shell fit to the first shell data of **2** refining ΔE_0, cn_O, cn_N, R_O, R_N, σ^2_O, and σ^2_N simultaniously (number of parameters = 7, N_{free} = 8) are as follows: $cn_O/R_O = 0.991$; $cn_O/R_N = 0.991$; $cn_O/\sigma^2_O = 0.987$; $cn_O/\sigma^2_N = 0.960$; $cn_N/R_O = -0.991$; $cn_N/R_N = -0.990$; $cn_N/\sigma^2_O = -0.969$; $cn_N/\sigma^2_N = 0.981$; $cn_N/cn_O = -0.993$; $R_O/R_N = 0.996$; $R_O/\sigma^2_O = 0.974$; $R_O/\sigma^2_N = -0.959$; $R_N/\sigma^2_O = 0.969$; $R_N/\sigma^2_N = -0.964$; $\sigma^2_O/\sigma^2_N = -0.912$

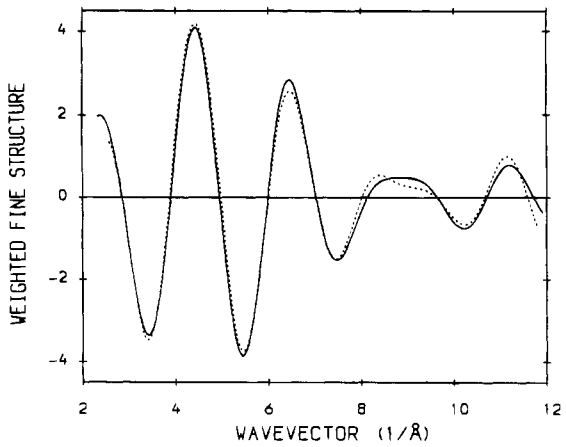

Figure 8. First shell data (—) and fit (•••) of **PAP7-Fe** (Fe K-edge).

the difference between the energy of the preedge peak and of an edge feature which originates from multiple scattering within the first shell (ΔE). According to Bianconi et al. ΔE depends on the mean absorber–scatterer distance (R_{av}) of the first shell.[43] Systematic analyses of suitable model compounds show that ΔE is a linear function of $1/R_{av}^2$.[36] The mean absorber–scatterer distances of the enzyme samples were determined with respect to the correlation derived from the model compounds. Details are described in ref 36.

Table 3 summarizes the results of the corresponding two-subshell fits to the first shell data of **PAP7-Fe**, **PAP7P-Fe**, **PAP4P-Fe**, and the model compounds. According to the preedge peak intensities the overall number of scatterers (Σcn) was set to 5 for **PAP7-Fe** and to 6 for **PAP7P-Fe** and **PAP4P-Fe**. The mean absorber–scatterer distances determined from the multiple scattering resonances in the XANES spectra of **PAP7-Fe**, **PAP7P-Fe**, and **PAP4P-Fe** are 2.00, 2.06, and 2.06 Å.[36,44] The mean absorber–scatterer distance in the native enzyme has the same order of magnitude as the corresponding distances in other five-coordinated complexes, e.g. in [Fe(saloph)catH] (1.966 Å) which contains a Fe(III) ion coordinated by five N/O donor atoms.[45] On the other hand, the mean absorber–scatterer distances found for **PAP7P-Fe** and **PAP4P-Fe** agree with the corresponding distance of **5-Fe** (R_{av} = 2.064 Å) which contains a μ-diphenylphosphato-bridged Fe(III)–Zn(II) core.[27] In addition, these values are in good agreement with the shifts of the first peak positions in the Fourier transform of the enzyme samples at the iron K-edge toward higher distances upon addition of phosphate.

For the native enzyme (**PAP7-Fe**) 2.4 O/N at an average distance of 1.91 Å and 2.6 O/N at 2.10 Å were found. As an example, Figure 8 shows the first shell EXAFS data and the result of the curve fitting analysis of **PAP7-Fe**. After addition of phosphate at pH 7 (**PAP7P-Fe**) the first shell EXAFS data could best be fitted with 2.4 O/N at 1.94 Å and 3.6 O/N at 2.12 Å. These values are in accordance with the corresponding absorber–scatterer distances reported for the oxidized forms of uteroferrin and bovine spleen PAP in the presence of phosphate (1.96 and 2.10 Å, and 1.98 and 2.13 Å, respectively).[8a,d]

Table 4. Results of Curve Fitting Analysis of the First Shell EXAFS Data of the Kidney Bean PAP (Zn K-Edge)

sample	window width (Å)	N_{free}[a]	scatterer	cn[b]	R (Å)	$10^3\sigma^2$ (Å^2)	ΔE_0 (eV)	RF[a] (%)
PAP7-Zn	1.1–2.3	6	O	3.4[c]	1.97	2.3	8.8	21.9
			N	1.6	2.08	0.5		
PAP7P-Zn	1.1–2.0	5	O	4.0[d]	1.98	1.4	6.0	24.2
			N	2.0	2.11	0.8		
PAP4P-Zn	1.2–2.0	4	O	4.7[d]	2.05	2.2	7.7	17.6
			N	1.3	2.18	0.8		
5-Zn	1.1–2.1	9	O	1.0[d]	2.04	1.2	7.9	16.0
			N	5.0	2.15	6.1		
6-Zn	1.0–2.1	10	O	1.6[d]	1.97	3.4	7.0	13.4
			N	4.4	2.12	6.2		

[a] As defined in the Experimental section. [b] cn = coordination number. [c] Σcn = 5. [d] Σcn = 6.

At lower pH values (**PAP4P-Fe**) the curve fits result in 2.8 O/N at 1.97 Å and 3.2 O/N at 2.19 Å which might indicate a protonation of a ligand.

Attempts to fit the first shell EXAFS data with a model involving a short (<1.8 Å) iron-μ-oxo scattering contribution (three subshells: Fe–μ-O, Fe–O, and Fe–N) did not succeed. The mean distance of this subshell always increases during the least squares fit procedures finally matching the mean absorber–scatterer distance found for the second subshell (Fe–O). Therefore, we assume that no μ-oxo bridges are present in the proteins.

Zinc K-Edge. The first shell data of the enzyme samples at the zinc K-edge were analyzed differently to the procedure described above: Due to the absence of a preedge peak it was impossible to determine R_{av} from the XANES spectra. Instead, two-subshell fits were performed according to ref 46. To avoid problems with the restricted number of free variables, the sum of the coordination numbers of the subshells has been fixed according to the values established from the XANES spectra. The results are summarized in Table 4. According to Eggers-Borkenstein et al.[46] the accuracy of the fit results obtained this way is ±0.04 Å with respect to the distances and ±25% with respect to the coordination numbers.[46]

Second and Third Shells. Native Enzyme. The main emphasis in analyzing the higher shell EXAFS data was put on the determination of the iron–zinc distance. Figure 9 compares the Fourier transform of **PAP7-Fe**, **1**, and **6-Fe**. **1** contains a homodinuclear Fe(III)–Fe(III) core with a metal–metal distance of 3.926 Å.[27] The Fourier transform of **1** is composed of scattering contributions from atoms in the first (3 O at 1.919 Å, 3 N at 2.171 Å), second (6 C at 3.015 Å) and third (1 Fe at 3.926 Å) shell. Due to the limited k range, the features in the Fourier transformed spectrum of **PAP7-Fe** are less intensive and broader than the peaks of **1**. Nevertheless, both Fourier transforms show great similarities. In particular, the peak at ca. 3.6 Å in the Fourier transform of **PAP7-Fe** is nearly equivalent to the metal–metal vector in the Fourier transform of **1**. Model compounds with shorter metal–metal distances (e.g. 3.436 Å for **6**) show characteristic features in their Fourier transformed spectra which are not observed for the native enzyme.

For dinuclear model compounds, the second shell normally contains a large number of C atoms (e.g. 10 for **6-Fe**) spread around 3.0 Å, always shorter than, and independent of, the metal–metal distance. Carbon shells at greater distances contribute less distinctly to the EXAFS because they are

(43) Bianconi, A.; Fritsch, E.; Calas, G.; Petiau, J. *Phys. Rev. B* **1985**, *32*, 4292.

(44) (a) Priggemeyer, S.; Eggers-Borkenstein, P.; Rompel, A.; Krebs, B.; Henkel, G.; Witzel, H.; Körner, M.; Nolting, H.-F.; Hermes, C. *X-ray Absorption Fine Structure*; Hasnain, S. S., Ed.; Ellis Horwood 1991; p 131. (b) Priggemeyer, S.; Rompel, A.; Eggers-Borkenstein, P. Krebs, B.; Henkel, G.; Nolting, H.-F.; Hermes, C.; Körner, M.; Witzel, H. *J. Inorg. Biochem.* **1991**, *43*, 543.

(45) [Fe(saloph)catH] = [*N,N'*-(1,2-phenylene)bis(salicylidenaminato)]-(catechol-*O*)iron(III). Heistand, R. H., II; Roe, A. L.; Que, L., Jr. *Inorg. Chem.* **1982**, *21*, 676.

(46) Eggers-Borkenstein, P.; Priggemeyer, S.; Krebs, B.; Henkel, G.; Simonis, U.; Pettifer, R. F.; Nolting, H.-F.; Hermes, C. *Eur. J. Biochem.* **1989**, *186*, 667.

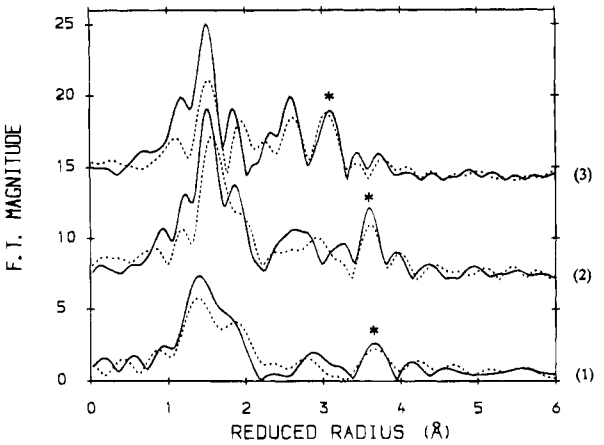

Figure 9. Fourier transform of the k^3-weighted fine structure (Fe K-edge) of **PAP7-Fe** (1), **1** (2), and **6-Fe** (3): solid line, Fourier transform range $2.5 < k < 11.5$ (16.9) Å^{-1}; dotted line, Fourier transform range $5.0 < k < 11.5$ (16.9) Å^{-1}. The metal−metal peaks are indicated by asterisks.

expected to have high static and thermal disorder. The metal−metal peak in the Fourier transform of **1** includes such scattering contributions of some low-Z atoms (carbon, oxygen, and nitrogen). In order to determine metal−metal distances it is necessary to separate the metal signal from scattering contributions of the low-Z atoms. According to different amplitude and phase dependences on k,[34,47] low-Z signals can be suppressed by Fourier transforming only k values greater than 5.0 Å^{-1} (dotted curve in Figure 9).[48] Figure 9 shows that the shapes of the metal peaks of **1** and **6-Fe** are less affected upon restriction of the Fourier transform range. The peak at 3.6 Å in the Fourier transform of **PAP7-Fe** exhibits the same characteristics suggesting the assignment of the peak to a metal signal as well.

The peak at ca. 3.6 Å in the Fourier transform of **PAP7-Fe** was Fourier filtered over the restricted data range (k_{min} = 5.0 Å^{-1}) and fitted with a one-shell model involving scattering contributions of a single zinc atom. Fits were performed varying ΔE_0, R_{Zn}, cn_{Zn}, and $\Delta\sigma^2_{Zn}$ (N_{free} = 4, see Table 5).

In the Fourier transform of **PAP7-Zn** the third peak is relatively broad and not well separated from the second shell peak particularly upon reducing the Fourier transform range. Therefore, both peaks were filtered over the original data range and fitted with a two-shell model involving Zn−C and Zn−Fe scattering contributions. Fits were performed varying ΔE_0,[49] cn_C, R_C, σ^2_C, R_{Fe}, and σ^2_{Fe} (N_{free} = 11, see Table 5). To avoid correlations, cn_{Fe} was fixed to one.

It is well-known that it is difficult to obtain unique fit results when fitting higher shell EXAFS data of dinuclear metalloproteins with a two-shell model involving metal−carbon and metal−metal scattering contributions. Nevertheless, this is only true for metalloproteins in which the second shell scatterers (normally carbon) are at radial distances near that of the metal−metal separation.[50,51] Since the carbon and iron subshells of **PAP7-Zn** are separated by 0.63 Å, no destructive interferences can be expected. Even for smaller differences in the mean absorber−scatterer distances reliable fit results can be obtained by the fit procedure described above (see fit result for **4**, Table 4).

Table 5. Results of Curve Fitting Analysis of the Higher Shell EXAFS Data of the Kidney Bean PAP (Fe and Zn K-edge)

sample	window width (Å)	N_{free}[a]	scatterer	cn[b]	R (Å)	$10^3\sigma^2$ (Å^2)	ΔE_0 (eV)	RF[a] (%)
PAP7-Fe	2.5−3.1	4	C	5.1	3.25	10.5	6.9	18.8
	3.2−4.1[c]	4	Zn	1.0	3.99	5.1	−0.1	8.8
PAP7P-Fe	3.1−3.9[c]	4	Zn	1.3	3.67	10.8	15.5	16.0
PAP4P-Fe	3.1−3.9[c]	4	Zn	1.6	3.71	9.2	13.5	13.1
PAP7-Zn	2.5−3.3	5	C	4.4	3.30	3.3	8.3	13.6
	2.5−4.0	9	C	4.1	3.30	2.1	8.5	9.9
			Fe	1.0[d]	3.93	3.6	0.2	
PAP7P-Zn	3.1−4.0[c]	4	Fe	0.7	3.71	1.0	18.9	10.1
PAP4P-Zn	2.8−3.9	6	C	6.0	3.38	3.5	11.4	23.3
			Fe	1.0[d]	3.69	5.4		
1	3.3−3.9[c]	5	Fe	0.8	3.94	2.3	−3.7	21.1
4	2.2−3.4	11	C	5.6	3.03	3.3	3.8	20.8
			Fe	1.0[d]	3.32	3.8		
5-Fe	3.1−3.8[c]	5	Zn	1.4	3.70	5.6	8.3	10.0
6-Fe	2.8−3.4[c]	5	Zn	0.8	3.39	2.3	−3.3	14.4
5-Zn	3.0−3.7[c]	6	Fe	0.6	3.68	1.9	1.8	17.2
6-Zn	2.8−3.4[c]	4	Fe	0.9	3.42	5.4	5.2	15.0

[a] As defined in the Experimental Section. [b] cn = coordination number. [c] Fourier transform: k_{min} = 5 Å^{-1}. [d] Not varied.

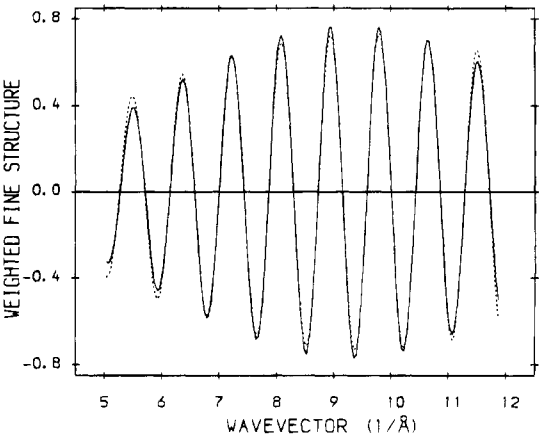

Figure 10. Third-shell data (iron−zinc scattering contribution) (—) and fit (···) of **PAP7-Fe**. Fourier transform range $5.0 < k < 11.5$ Å^{-1}.

In order to make sure that the second peaks in the Fourier transform of **PAP7-Fe** and **PAP7-Zn** include no metal−metal scattering contribution both peaks were Fourier-filtered exclusively and modeled with a single carbon shell (see Table 4). As expected, addition of an iron−zinc or zinc−iron scattering contribution does not improve the fit results.

The iron and zinc sites of the dimetal core of the kidney bean PAP can be analyzed independently enabling a mutual check of the metal−metal distances determined from the EXAFS data. The iron−zinc distance obtained from the iron EXAFS is 3.98 Å, from the zinc EXAFS 3.93 Å (see Figures 10 and 11). Comparison of the curve fitting results for suitable model compounds with the structural data obtained by X-ray crystallography shows that the error of metal−metal distances extracted from EXAFS data using the procedure above is at least ±0.05 Å.[36] Therefore, both metal−metal distances agree within the accuracy normally obtained with EXAFS spectroscopy. In the subsequent discussion the mean value of 3.96 Å will be used.

In general, peaks around 4 Å in Fourier-transformed spectra can also arise from the scattering contribution of third shell C

(47) (a) Teo, B.-K.; Lee, P. A. *J. Am. Chem. Soc.* **1979**, *101*, 2815. (b) Teo, B.-K.; Lee, P. A.; Simons, A. L.; Eisenberger, P.; Kincaid, B. M. *J. Am. Chem. Soc.* **1977**, *99*, 3854.
(48) Zhang, K.; Stern, E. A.; Ellis, P.; Sanders-Loehr, J.; Shiemke, A. K. *Biochemistry* **1988**, *27*, 7470.
(49) In order to obtain optimal transferability of the amplitude and phase functions one ΔE_0 for each subshell was allowed to vary.
(50) Hedman, B.; Co, M. S.; Armstrong, W. H.; Hodgson, K. O.; Lippard, S. J. *Inorg. Chem.* **1986**, *25*, 3708.
(51) Scott, R. A.; Eidsness, M. K. *Comments Inorg. Chem.* **1988**, *7*, 235.
(52) (a) Strange, R. W.; Blackburn, N. J.; Knowles, P. F.; Hasnain, S. S. *J. Am. Chem. Soc.* **1987**, *109*, 7157. (b) Co, M. S.; Scott, R. A.; Hodgson, K. O. *J. Am. Chem. Soc.* **1981**, *103*, 986.

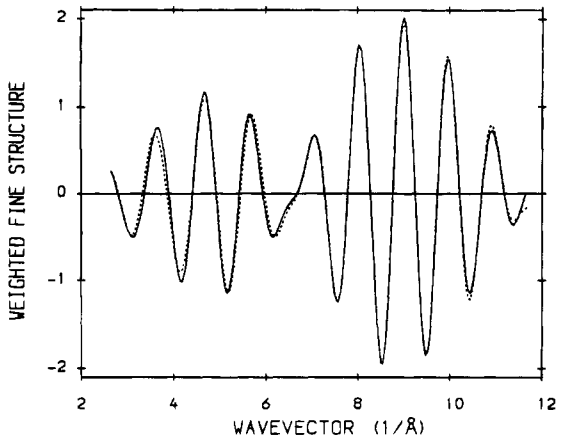

Figure 11. Second- and third-shell data (—) and fit (•••) of **PAP7-Zn** (1) (zinc–carbon and zinc–iron scattering contribution).

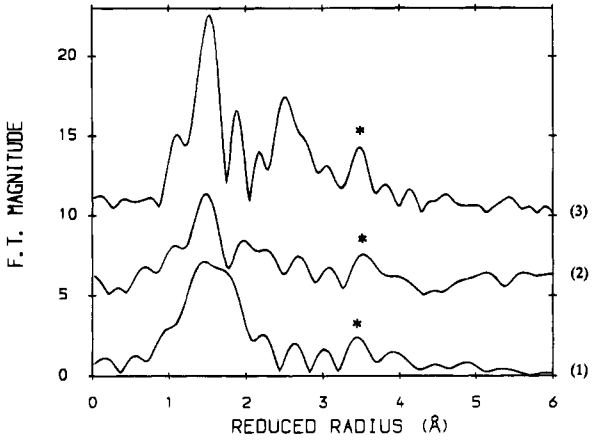

Figure 12. Fourier transform of the k^3-weighted fine structure (Fe K-edge) of **PAP7P-Fe** (1), **PAP4P-Fe** (2), and **5-Fe** (3). The asterisks indicate the iron–zinc peaks.

and N atoms from histidine ligands enhanced by multiple scattering pathways.[52] However, a recent EXAFS investigation of reduced uteroferrin with a related ligation of the metal sites clearly demonstrates that multiple scattering contributions can be neglected.[8d]

Addition of Phosphate. Figure 12 compares the Fourier-transformed spectra of **PAP7P-Fe** and **PAP4P-Fe** with the heterodinuclear complex **5-Fe**. Since **5-Fe** is a highly symmetric complex (low preedge peak intensity) with a compact three-dimensional structure, different intensities for the peaks between 1 and ca. 3 Å in the Fourier-transformed spectra of the enzyme samples and **5-Fe** are not unexpected (note that the second peak in the Fourier transform of **5-Fe** results from scattering contributions of 8 C and 2 P atoms). However, the peaks at ca. 3.4 Å in the Fourier transform of **PAP7P-Fe** and **PAP4P-Fe** and the iron–zinc vector of **5-Fe** are nearly equivalent, suggesting the assignment of the peaks to the metal–metal peak as well.

Therefore, the peaks were Fourier-transformed for k values greater than 5 $Å^{-1}$, Fourier-filtered with window widths as indicated in Table 5, and fitted with a one-shell model as described for **PAP7-Fe**. Consequently, the corresponding (fourth) peak in the Fourier transform of **PAP7P-Zn** (see Figure 7)—which had to include the metal–metal scattering contribution as well—was analyzed the same way. This procedure, however, was not feasible for **PAP4P-Zn** since the resolution of the third and fourth peak in the Fourier-transformed spectra was insufficient. In this case, both peaks were Fourier-filtered over the original data range and fitted with a two-shell model as described for **PAP7-Zn**.

The iron–zinc distances of **PAP7P** determined this way are 3.67 Å (**PAP7P-Fe**) and 3.71 Å (**PAP7P-Zn**). Both metal–metal distances agree within the accuracy usually obtained with EXAFS spectroscopy. Therefore, a mean iron–zinc distance of 3.69 Å can be assumed. The corresponding metal–metal distances of **PAP4P** are in good agreement (R = 3.67 Å and 3.69 Å, respectively) and result in a mean iron–zinc distance of 3.68 Å.

In order to analyze the M–P scattering contribution the second peak in the Fourier-transformed spectra of **5** at the Fe and Zn K-edge was Fourier-filtered. According to the structural parameters of **5**, we tried to fit the Fourier-filtered fine structure with a two shell model containing M–C and M–P (M = Fe, Zn) scattering contributions. Such fits, however, always resulted in unreasonable coordination numbers (if c_{NP} was allowed to vary) and/or Debye–Waller factors (particularly negative values) and/or absorber–scatterer distances for the phosphorus subshell. The same situation was found when fitting the second and third peaks in the Fourier transformed spectra of **PAP7P** and **PAP4P** at the Fe and Zn K-edge. Although it is most likely that phosphorus atom(s) contribute to the EXAFS in this domain, reliable fit results could not be reproduced for the phosphorus subshell. This might be due to a destructive interference of the scattering contributions of the phosphorus and carbon subshell. As mentioned before, similar interferences have already been described for the scattering contribution of carbon and metal atoms at nearly the same distance.

Discussion

Native Enzyme. X-ray absorption analyses confirm the presence of a dinuclear Fe(III)–Zn(II) center in the active site of the enzyme. Iron and zinc are coordinated by N/O donor ligands. No evidence was found for the involvement of a heavier atom (e.g. sulphur from cysteine) in the first shell EXAFS data. Analyses of the XANES regions reveal both ions to be five-coordinated in the native enzyme. In this respect, the native kidney bean PAP differs from the active sites of uteroferrin and the bovine spleen PAP, which were reported to be composed of six-coordinated iron ions.[8a,8d] The additional ligand might be a water molecule. The pentacoordination of the zinc site might be the reason that Zn(II)—if compared with Fe(II) or Co(II)—is much faster incorporated into the zinc-depleted semiapoenzyme.[53]

EXAFS spectroscopy normally provides no information about the nature of the ligands. A tyrosine ligand has to be postulated at the Fe(III) site due to the CT-band. Furthermore, a histidine at the Zn(II) site has to be postulated since the Zn-depleted semiapoenzyme can not be reconstituted with Zn after treatment with diethyl pyrocarbonate. Nevertheless, this is possible after reaction with hydroxylamine.[52]

The iron–zinc distance of the native enzyme was determined to be 3.96 Å. This value is greater than the metal–metal distances reported for other enzymes also containing a dinuclear center like the mammalian PAPs, hemerythrin,[54] ribonucleotide reductase,[55] or methane monooxygenase.[56] For the active

(53) (a) Körner, M. Ph.D. Dissertation, University of Münster, 1992. (b) Körner, M.; Witzel, H. to be published.
(54) (a) Stenkamp, R. E; Sieker, L. C.; Jensen, L. H. *J. Am. Chem. Soc.* **1984**, *106*, 618. (b) Sheriff, S.; Hendrickson, W. A.; Smith, J. L. *J. Mol. Biol.* **1987**, *197*, 273.
(55) Nordlund, P.; Sjöberg, B.-M.; Eklund, H. *Nature* **1990**, *345*, 593.
(56) DeWitt, J. G.; Bentsen, J. G.; Rosenzweig, A. C.; Hedman, B.; Green, J.; Pilkington, S.; Papaeftymiou, G. C.; Dalton, H.; Hodgson, K. O.; Lippard, S. J. *J. Am. Chem. Soc.* **1991** *113*, 9219.

(reduced) diiron form of the bovine spleen PAP an iron–iron distance of 3.0–3.2 Å was estimated.[8a] However, a longer metal–metal distance of 3.52 Å which has been reported recently seems to be more likely for the Fe(III)–Fe(II) species of the mammalian PAP's.[8d] Even the iron–iron distance in methemerythrin is about 3.2 Å and increases upon reduction to the Fe(II)–Fe(III) form by ca. 0.2 Å to 3.42 Å.[48,57] In addition, the metal–metal separations found for synthetic (μ-phenoxo)-bis(μ-carboxylato)-bridged M(II)–Fe(III) (M = Zn, Fe) complexes are in the same order as those determined for the hemerythrin derivatives.[1a,58] The large iron–zinc distances found in this work, therefore, cannot support the existence of a triply bridged iron–zinc core in the native enzyme. Summarizing the combined EXAFS results together with conclusions from previous investigations[53a] lead us to propose the following general structural scheme for the active dinuclear site in our samples of the native enzyme (**PAP7-Fe**):

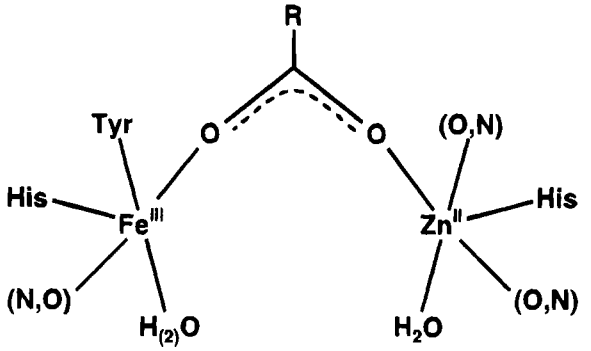

Nevertheless, the exchange of Zn(II) by Fe(II) in the kidney bean enzyme might lead to a shorter distance. However, a μ-oxo bridge in the oxidized diiron species of the kidney bean enzyme—which is still in discussion for the Fe(III)–Fe(III) derivatives of the PAP's—seems to be unlikely since the ΔE_Q values in the corresponding Mössbauer spectra of the kidney bean derivative are too small for μ-oxo bridges.[17]

Unfortunately, EXAFS spectroscopy normally provides no information about the presence of other bridging ligands. However, the absence of an EPR signal in the Fe(III)–Fe(III) species of the kidney bean PAP and the appearance of a new signal at $g_{av} = 1.75$ after reduction to the Fe(III)–Fe(II) form[12] strongly indicates that both iron ions are antiferromagnetically coupled, comparable to the situation in uteroferrin and the bovine spleen PAP.[3,9c] These magnetic interactions are also found in the Mössbauer spectra of the Fe–Fe kidney bean derivative.[17] Therefore, at least one bridging ligand has to be postulated. This might be a carboxylato group from aspartate in the Fe(III)–Fe(II) enzyme or a hydroxo ligand which may bind to the sixth coordination site not occupied in the native enzyme. Further EXAFS studies on the Fe(II)-substituted kidney bean enzyme should help to clarify these questions.

Interaction with Phosphate. The effect of phosphate on the PAP's has been the subject of some controversy. Though the M–P (M = Zn, Fe) scattering contribution could not be analyzed, information about how phosphate interacts with the dimetal core of the kidney bean PAP can be obtained by analyzing the changes in the first coordination spheres of the ions and in the metal–metal distances upon addition of phosphate.

The addition of phosphate to the native enzyme at a pH-value of about 7 results in an increase of the coordination number from five to six at both the iron and zinc K-edges. Also, the mean absorber–scatterer distance of the first coordination shell at the iron K-edge increases from 2.00 to 2.06 Å. On the other hand, the metal–metal distance decreases by 0.27 Å to 3.69 Å. On the basis of these facts, we assume an O,O'-bridging mode of the phosphate anion in the kidney bean enzyme. It is most likely that phosphate binds to both the iron and zinc ion occupying the free coordination site and thereby contracts the distance between the metal ions. Other possibilities, e.g. coordination to only one of the metal ions or bonding of phosphate to the protein close to but not directly to either metal ion, are very unlikely because of the dramatic decrease of the metal–metal distance. The resulting metal–metal distance is in good agreement with the metal–metal distances found for **5** and the analogous (μ-phenoxo)bis(μ-diphenylphosphato)-bridged Fe(III)–Fe(II) compound $[Fe_2(bpmp)(dp)_2](ClO_4)_2$.[27] It is not unusual that metal–metal distances are dependent on the bite distances of bridging ligands. For example, **5** and $[Fe_2(bpmp)(dp)_2](ClO_4)_2$ have metal–metal distances of 3.695 and 3.649 Å whereas the metal–metal distances of the corresponding μ-carboxylato-bridged species, **6** and $[Fe_2(bpmp)(OPr)_2](BPh_4)_2$, are 3.436 and 3.365 Å.[27,28]

True et al. analyzed the higher shell EXAFS data of the phosphate- and arsenate-bound forms of the oxidized uteroferrin.[8d] They determined iron–phosphorus and iron–arsenic distances of 3.17 and 3.41 Å, respectively, and observed an iron–iron distance of 3.2–3.3 Å for both derivatives. On the basis of their analysis they supposed a bidentate bridging coordination mode of the oxoanions. Although **PAP7P** has to be compared with the reduced form of uteroferrin in the presence of phosphate (or arsenate), phosphate anions seem to interact with the dimetal center of both proteins in the same way.

Lowering the pH value only affects the first coordination sphere of the iron as well as the zinc ion. A comparison of the Fourier-transformed spectra of the kidney bean PAP shows that peaks arising from scattering atoms in higher shells remain essentially unchanged. Nearly the same iron–zinc distances were found for both pH 7 and pH 4. However, the first coordination spheres of the iron and zinc ions in **PAP4P** became more distorted.

At lower pH protonation of a ligand is most likely. The protonated ligand should form weaker bonds to the metal ions resulting in longer absorber–scatterer distances and therefore in a more distorted geometry. A OH^-/H_2O equilibrium at the Fe(III) ion in the bovine spleen PAP with a pK value around 4.5 has been proposed based on the pH dependence of the enzymatic activity and on spectroscopic properties of the bovine spleen PAP.[3e,g] This equilibrium would be reflected in the first coordination sphere of the iron ion and would be in agreement with the observed distortion of the first shell at lower pH values.

Since the structure of the higher shells, particularly the iron–zinc distance, is maintained upon lowering the pH value—especially when compared to the structural changes caused by addition of phosphate—a bridging coordination mode of the phosphate anion is not affected by the protonation of one oxygen atom.

Acknowledgment. Financial support from the Bundesminister für Forschung und Technologie, from the Deutsche Forschungsgemeinschaft, and from the Fonds der Chemischen Industrie is gratefully acknowledged.

IC940112P

(57) Scarrow, R. C.; Maroney, M. J.; Palmer, S. M.; Que, L., Jr.; Roe, A. L.; Salowe,S. P.; Stubbe, J. *J. Am. Chem. Soc.* **1987**, **109**, 7857.
(58) Kurtz, D. M., Jr. *Chem. Rev.* **1990**, *90*, 585.